BUILDING DAMAGE DETECTION FROM POST-EARTHQUAKE AERIAL IMAGES USING WATERSHED SEGMENTATION IN GOLCUK, TURKEY

E. Sumer [a], M. Turker [b]

[a] Baskent University, Department of Computer Engineering, Eskisehir Road 20.km 06530 Ankara, Turkey – esumer@baskent.edu.tr

[b] Middle East Technical University, Graduate School of Natural and Applied Sciences, Geodetic and Geographic Information Technologies, 06531, Ankara, Turkey – mturker@metu.edu.tr

Commission VII, WG VII/5

KEY WORDS: Remote Sensing, Earthquakes, Detection, Segmentation, Aerial, Edge, Urban, Building.

ABSTRACT:

The collapsed buildings due to earthquake were detected from post-event aerial images using watershed segmentation algorithm. The objective was to detect the collapsed buildings based on the analysis of the cast shadows. The building boundaries were available and stored in a GIS as vector polygons. The building polygons were utilized to perform assessments in a building specific manner. The approach was implemented in a selected urban area of Golcuk. The shadows cast by the buildings were detected using the watershed segmentation algorithm. The shadow casting edges of the buildings were identified and a buffer zone was generated for each building polygon along these edges. Then, the initial points falling within the buffer zone were selected from both inside and outside the building polygons to start the watershed segmentation. The shadow regions were detected using a watershed segmentation algorithm. This was followed by measuring the agreement between the shadow producing edges of the buildings and the corresponding shadows based on the percentage of the shadow pixels. Of the 284 buildings analyzed, 229 were correctly labeled as collapsed or un-collapsed providing an overall accuracy of 80%. The results prove that the collapsed buildings caused by the earthquake can be successfully detected from post-event aerial images.

1. INTRODUCTION

An earthquake, an unpredictable and unpreventable event, is regarded as one of the most destructive natural disasters on earth. On 17 August 1999, the urban areas of Golcuk, Yalova, Izmit and Istanbul were significantly damaged by an earthquake. It is estimated that 50,000 buildings were heavily damaged, over 15,000 people died and about 32,000 people were injured in this dreadful event. The epicenter of the earthquake was 40.70^{o} N, 29.91^{o} E (USGS), near the city of Izmit. The magnitude and the depth were 7.4 and 20 km respectively. The region struck by the earthquake, accommodates nearly 20% of the total population and is the most industrialized zone of Turkey.

The extent of the damage caused by this catastrophic event needs to be assessed rapidly in order to reduce its effects by setting the corresponding agencies in motion. This can be efficiently performed using remote sensing technology that provides up-to-date information about the earth surface features. Change detection approaches can be used to detect the earthquake-induced changes using the pre- and post-quake aerial photographs or satellite images by comparing and analyzing them. There are also several other methods for collecting information on damage due to earthquakes such as field surveys, aerial television imagery, and satellite imagery (Hasegawa *et al*., 1999).

The objective of this study is to determine the collapsed buildings in a selected urban area of Golcuk using a watershed segmentation algorithm. A shadow-based damage detection method was proposed. The implementation of the approach was carried out using MATLAB® 6.5 which is a high-performance language for technical computing.

2. PREVIOUS STUDIES

In many applications of damage assessment and building detection, the aerial photography is widely used due to its advantages such as improved vantage point, permanent recording, broadened spectral sensitivity, the increased spatial resolution, and geometric fidelity. One of the frequently used applications of aerial photography is the detection of the buildings from their shadows. Irvin *et al.,* (1989) states that the shadows are usually among the darkest areas in images and their extraction can be feasible using image processing techniques. They developed several methods to estimate the grouping of related structures together with the shape, verification and height of individual structures. In each method, the main approach used was the relation between structures and their cast shadows. Another study concerning building shadows was realized by Huertas *et al.,* (1988). They used building shadows to estimate the building heights. In addition, the shadows cast by the buildings were utilized in verification of the buildings. Their method was comprised of four steps including line and corner detection, labeling of the corners based on shadows, tracing of object boundaries, and finally the verification of hypotheses.

Ishii *et al.,* (2002) proposed a method, containing two cases, to detect the damaged areas from aerial photographs. In the first case, color and edge information were used to detect the damaged areas from a post-quake aerial photograph. Combining the color information with the edge information, the

discrimination of the damaged areas from the non-damaged could be done successfully. In the second step, aerial photographs of the same area taken before and after the earthquake were available. They matched the two images by using the affine transform and also by hand. Then, the colors of the corresponding pixels in each image were checked. Thus, the areas having color differences were examined. As a consequence, the two-case method were said to be fairly good in determining the damaged areas. A similar study was conducted by Mitomi *et al.,*(2000) who detected the damaged buildings by processing the aerial television images taken after the 1999 Kocaeli, Turkey and Chi-Chi, Taiwan earthquakes. The method was composed of defining the characteristics of damage to wooden buildings based on hue, saturation, brightness and the edge elements. Firstly, the damaged and non-damaged pixels were classified. Then, texture analysis was carried out and the damaged buildings were identified.

A near-real time earthquake damage assessment using the integration of GIS and remote sensing was performed by Gamba *et al.,* (1998). Their approach was comprised of two phases. In the first phase, GIS side of the study was performed via collecting and analyzing data about buildings and infrastructures. In the second phase, the system receives near-real time imagery of the suffered area to perform change detection through shape analysis and perceptual grouping using the pre and post-event aerial images.

Turker and San (2003) used pre- and post-event SPOT HRV images to detect the Izmit earthquake induced changes. The change areas were detected by subtracting the near-infrared channel of the merged pre-event image from that of the post-event image. The overall accuracy for the change areas were found to be 83%.

In a recent study, Turker and Cetinkaya (in press), detected the collapsed buildings caused by the 1999 Izmit, Turkey earthquake using digital elevation models (DEMs) created from the aerial photographs taken before (1994) and after (1999) the earthquake. The DEMs created from two epochs were differenced and the difference DEM was analyzed on a building-by-building basis for detecting the collapsed buildings. The producer's accuracy for collapsed buildings was computed as 84%. Further, Turker and San (in press) utilized the cast shadows to detect the collapsed buildings due to Izmit, Turkey earthquake. The available vector building boundaries were used to match the shadow casting edges of the buildings with their corresponding shadows and to perform analysis in a building specific manner. Of the 80 collapsed buildings, 74 were detected correctly, providing 92.50% producer's accuracy.

In the present case the earthquake-damaged buildings are detected from post-event aerial images using watershed segmentation. This segmentation is based on the concepts of watersheds and catchment basins, which are well known in topography. In this approach, a gradient image can be regarded as a topographic surface where the gray-levels of the gradient image represent altitudes. (Figure 1). Therefore, the edges in the image having high brightness values are considered as watershed lines while the interior regions of the image having low brightness values can be considered as catchment basins (Sonka et al.,1998). The first step of the segmentation is finding the minima (catchment basin) and piercing of it. Then, whole relief is immersed into the water that causes the water flooding into the areas close to the piercing points. As the relief goes deeper in the water, some flooded areas tend to merge. In order to prevent this, infinitely tall dams are placed along the watershed lines. At the end, the resulting group of dams defines the watersheds of the image (Shafarenko *et al.,* 1997). Vincent *et al.,*(1991) developed a fast and flexible algorithm for computing watersheds in digital grayscale images. The algorithm is based on an analogy of an immersion process. In this algorithm, the flooding of the water in the image is efficiently simulated using a queue of pixels. They applied the algorithm in several fields with regard to picture segmentation including MR imagery and digital elevation models.

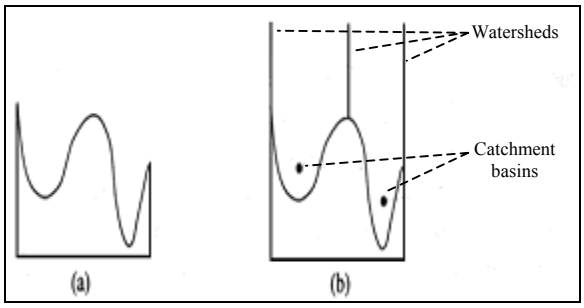

Figure 1. Watershed segmentation in one dimension: (a) gray-level profile of the image data; (b) watershed segmentation – local minima of gray level (altitude) yield catchment basins; local minima define the watershed lines.

3. STUDY AREA AND DATA

3.1 Study Area

A selected urban area of the city of Golcuk was used as the study area (Figure 2). A post-quake panchromatic aerial photograph (1m resolution) of the region was obtained from General Command of Mapping of Turkey. The study area consists of 284 rectangular shaped buildings. Of the 284 buildings, 79 were collapsed and the remaining 205 buildings were un-collapsed. The vector building boundaries were available from a previous study conducted by San (2002) in our department. The data contains for each building the Cartesian coordinates of the edge points.

Figure 2. Study Area

3.2 Methodology

The main steps followed in the proposed damage assessment method are illustrated in Figure 3. First, the post-event aerial photograph of the area was pre-processed using histogram equalization technique to provide better discrimination between the buildings and their shadows. Next, the buildings were selected one-by-one using the vector building boundary information. Then, for each building, the shadow-producing edges were determined. To do that, a simple algorithm was developed. The illumination angle was available from a previous study conducted by San (2002) as 135^{o} from the x-axis. A buffer zone was generated along the shadow edges of the buildings. This was followed by the execution of the watershed segmentation algorithm. For each building, a binary-colored output representing the shadow and non-shadow areas was generated. Finally, the accuracy assessment was carried out by comparing the analyzed buildings with the reference data.

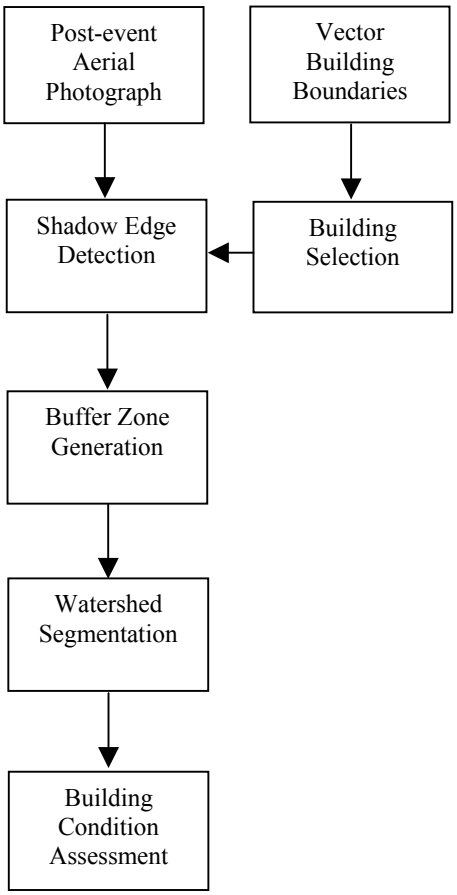

Figure 3. Damage detection using watershed segmentation

3.2.1 Building Selection and Shadow Edge Detection:

To select the vector building polygons, each polygon was assigned a unique identification code. In addition, the edges of each polygon were also given numerical codes. The edges and the corresponding (x, y) coordinates of a building (#175) are illustrated in figure 4. The labeling of the edges was necessary to identify the shadow casting edges of a building being assessed and to relate these edges with the corresponding shadows.

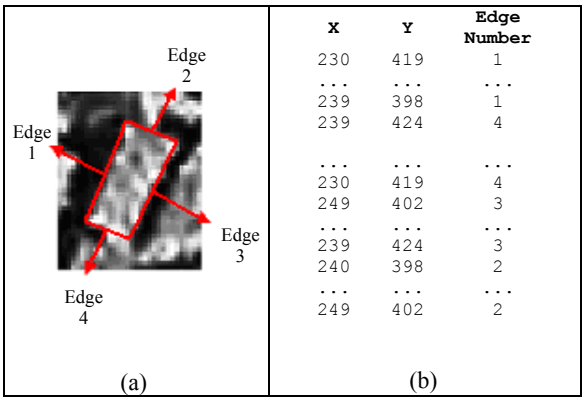

X	Y	Edge Number
230	419	1
...	...	...
239	398	1
239	424	4
...	...	...
230	419	4
249	402	3
...	...	...
239	424	3
240	398	2
...	...	...
249	402	2

Figure 4. (a) The edges of building #175 and (b) The format of vector data

After selecting a building, a minimum-bounding rectangle was generated using the vector information by finding the minimum and maximum x-y coordinates (totally four points). Then, these points were connected to each other and the minimum-bounding rectangle was constructed. A buffer bound was then generated via expanding the minimum-bounding rectangle from its edges about six pixels. The bound was created in order to take into account the shadow regions produced by the buildings. Next, the shadow producing edges of the selected building were detected using a simple algorithm. The algorithm works as follows. The corner points are found from the vector information. This is simply finding the points that share the same end point on adjacent edges. For example, since both edge 4 and edge 1 share the same end point, (x=230,y=419), this end point is selected as a corner point (Figure 4b). Then, the Euclidean distances (d_1, d_2, d_3, d_4), shown in figure 5a, are computed between the corner points of the building and the corner of the minimum-bounding rectangle in the illumination direction. The computed distances are then sorted. If there is only one maximum distance, the edges that contain the same corner point are selected as the shadow edges. If on the other hand, there are two maximum distances then, the edge that contains those corner points is the shadow edge. These two cases can be illustrated with an example. If $d_1 > d_4 > d_2 > d_3$, then the shadow edges are determined as edge 1 and edge 2 (figure 5b). This is because the corner point connecting these edges possesses the farthest distance (d_1). If the ranking is $d_1 = d_4 > d_2 > d_3$, then edge 1 is selected as the shadow edge since it is the only edge containing the farthest distances d_1 and d_4.

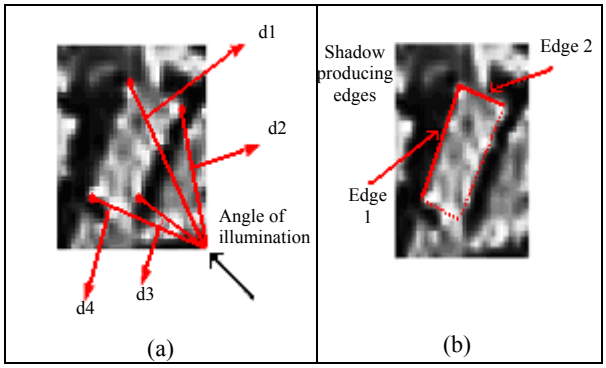

Figure 5. (a) The Euclidean distances and the angle of illumination. (b) The shadow producing edges of building # 175

3.2.2 Buffer Zone Generation:

A three pixel wide buffer zone was generated around the shadow producing edges of each building (figure 6). It was divided into two sub-zones (i) inside building, and (ii) outside building. The inside building part of the buffer zone (zone B) was used for building analysis while the outside building part of the buffer zone (zone S) was used for shadow analysis. The purpose of the buffer zone generation was to deal with the shadow and building areas around the shadow producing edges of the buildings. These areas can also be called 'the most significant parts' of a building for the damage assessment.

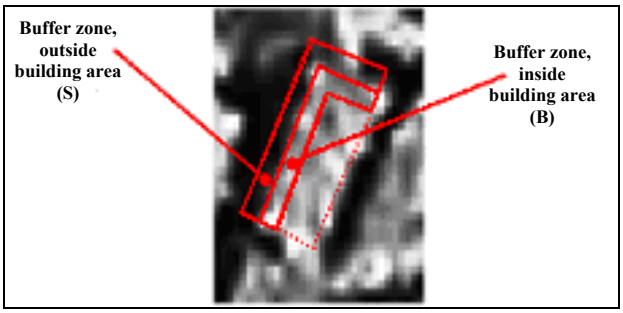

Figure 6. Buffer zone generation along the shadow producing edges

3.2.3 Watershed Segmentation:

The watershed segmentation was performed based on the idea of flooding from selected sources (Beucher *et al.,* 1992). These sources represent the markers. Two sets of markers were needed, one for shadow areas and the other for the building regions. These markers were utilized to avoid the over-segmentation. After the gradient image was found, the shadow and the building markers were selected within the outside building buffer zone (S) and the inside building buffer zone (B) respectively. The locations of the markers were seeded randomly. Figure 7a shows an example for the marker orientation on a gradient image.

The watershed segmentation algorithm was run to generate a binary image. After running the watershed algorithm, the two-region output image was obtained. Of these regions, one refers to shadow areas while the other corresponds to the building areas. In figure 7b, the shadow and the building areas are shown in blue and yellow colors respectively.

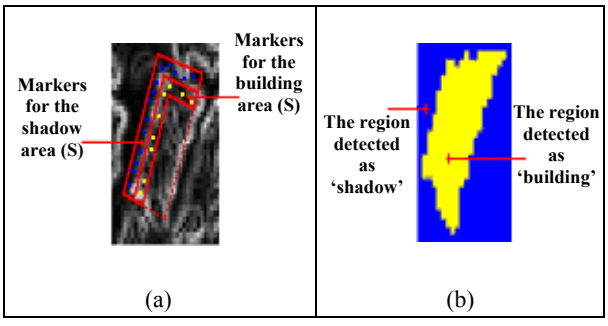

Figure 7. (a) The starting pixels (markers) for watershed transform, and (b) the segmented output after the watershed transform.

3.2.4 Assessing the Conditions of the Buildings:

After detecting the shadow and building areas, for each building, the agreement was measured within the buffer zone of the shadow producing edges between the pixels labeled as building and the pixels labeled as shadow (figure 8). To do that the pixels inside the shadow buffer (S) and the building buffer (B) were counted and categorized as shadow pixel or building pixel. Then, a ratio was computed between those pixels labeled as building and the total number of pixels falling inside the building of the buffer zone. Similarly, a ratio was also computed between those pixels labeled shadow and the total number of pixels falling inside the shadow region of the buffer zone. This can be illustrated with an example. The pixel distribution of building # 175 is shown in table 1. For this building, the shadow detection algorithm detected two shadow edges, which are 1 and 2. The total pixels inside the buffer zone along the shadow edges were calculated and labeled as "Total Assessed Pixels" (Table 1). Totally, 99 pixels were generated for shadow buffer and 99 pixels were generated for building buffer. After the watershed transform, 91 shadow pixels (blue pixels) fell into the shadow buffer and 66 building pixels (yellow pixels) fell into the building buffer. Then, the building and the shadow percentages were calculated as 66/99 = **66.67%** and 91/99 = **91.92%** respectively. A user-defined threshold was used to make a decision about the building. If the building ratio or the shadow ratio is below the threshold value, then the building is labeled as collapsed. If on the hand, both the building and the shadow ratios are over the threshold value then, the building is labeled as un-collapsed. The building and the shadow ratios were used together in deciding the building condition in order to reduce the misdetection of the buildings.

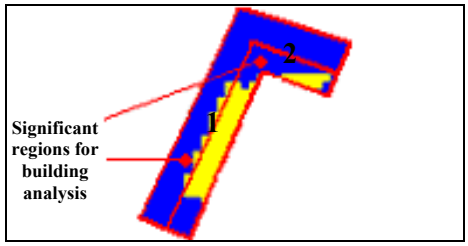

Figure 8. The regions used in the building analysis.

Total Assessed Pixels: 99
Detected Shadow Pixels: 91
Detected Building Pixels: 66
Shadow Ratio: 0.9192
Building Ratio: 0.6667

Table 1. Calculation of (building / shadow) pixel percentages.

3.3 Results

Table 2 provides the accuracy indices computed for the threshold values between 20% and 80%. These are overall accuracy, overall kappa, average user's accuracy, average producer's accuracy, combined user's accuracy and combined producer's accuracy. Of the six indices, four gave the highest percentage in the 50% threshold level. The remaining two indices did not reach to the maximum value at 50%. But, their percentages were not quite different from the maximum. For this reason, 50% level was chosen as the optimum threshold. The trend of the overall accuracies versus varying threshold values is also shown graphically in figure 9. It can be clearly seen in the

figure that the peak of the overall accuracy (80,63%) is reached when the threshold value is 50%.

Threshold (%)	Overall Accuracy (%)	Overall Kappa x 100	Average Accuracy		Combined Accuracy	
			User's	Producer's	User's	Producer's
20%	72,89	4,71	73,93	51,66	73,41	62,28
30%	76,06	22,24	77,40	58,52	76,73	67,29
40%	77,46	35,32	73,09	65,33	75,28	71,40
50%	80,63	51,19	75,93	75,30	78,28	77,97
60%	74,65	45,01	71,41	75,83	73,03	75,24
70%	64,08	32,98	68,15	72,01	66,12	68,05
80%	42,61	11,28	62,98	59,08	52,80	50,85

Table 2. The accuracy indices for the threshold values between 20% and 80%.

All the buildings contained within the study area were analyzed using the optimum threshold of 50%. An error matrix was generated by comparing the analyzed results with the reference data. The error matrix contains the overall accuracy, the user's, and the producer's accuracies for collapsed and un-collapsed buildings (Table 3). The overall accuracy (80,63%) was computed by dividing the sum of the diagonal of the error matrix (highlighted in gray) by the total number of the buildings (284). The producer's for collapsed, the producer's for un-collapsed, the user's for collapsed, and the user's for un-collapsed buildings were also computed as 63,29%, 87,31%, 65,79% and 86,06% respectively. It is evident that, 55 buildings were incorrectly detected. Of these buildings, 29 were not detected as collapsed through the analysis. Instead, 26 un-collapsed buildings were detected as collapsed. The mis-detected buildings represent the omission and commission errors respectively.

	Reference		
	Collapsed	Un-collapsed	Total
Collapsed	50	26	76
Un-collapsed	29	179	208
Total	79	205	284
Producer's	63,29	87,31	
User's	65,79	86,06	
Overall	80,63		

Table 3. Error matrix and accuracies

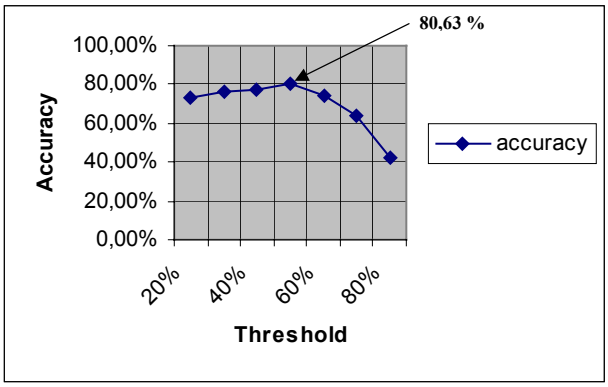

Figure 9. The change of the overall accuracy as the threshold changes.

4. CONCLUSIONS

In this study, we presented an approach for detecting the earthquake-damaged buildings through shadow analysis of the watershed segmented post-event aerial imagery. The approach was implemented in an urban area of the city of Golcuk. A total of 284 buildings were analyzed to measure their conditions. The results are quite encouraging. Of the 79 collapsed buildings, 50 were detected correctly providing a producer's accuracy of 63.29% and a user's accuracy of 65.79%. On the other hand, of the 205 un-collapsed buildings, 179 were labeled correctly providing a producer's accuracy of 87.31% and a user's accuracy of 86.06%. The overall accuracy was computed as 80.63%.

We found that determining the optimum threshold for separating the damaged buildings from non-damaged is important. In the present case the optimum threshold was computed as 50%. This threshold value is valid for this study only, and should not be considered global. The proposed method has several shortcomings to be improved in the future. The selection of the the initial markers is one problem. The buffer zones that are defined by the user can be expanded or shrinked to find a better aggreement between the shadow pixels (generated by the algorithm) and the actual shadow pixels.

REFERENCES

Beucher, S. and Meyer, F., 1992. The morphological approach of segmentation: the watershed transformation. In: *Mathematical Morphology in Image Processing*, E. Dougherty, Ed., chapter 12, pp. 433–481. Marcel Dekker, New York.

Gamba, P. and Casciati, F., 1998. GIS and Image Understanding for Near-Real-Time Earthquake Damage Assessment. *Photogrammetric Engineering and Remote Sensing*, 64(10), pp. 987-994.

Hasegawa, H., Aoki, H., Yamazaki, F. and Sekimoto, I., 1999. Attempt for Automated Detection of Damaged Buildings Using Aerial HDTV Images. *Proceedings of the 20th Asian Conference on Remote Sensing,* Vol. 1, pp. 97-102.

Huertas, A. and Nevatia, R., 1988. Detecting Buildings in Aerial Images. *Computer Vision, Graphics, and Image Processing*, 41(2), pp. 131-152.

Irvin, R.B., and McKeown, D.M., 1989. Methods for Exploiting the Relationship Between Buildings and Their Shadows in Aerial Imagery. *IEEE Transactions On Systems, Man, and Cybernetics*, 19(6), pp. 1564-1575.

Ishii, M., Goto, T., Sugiyama, T., Saji, H. and Abe, K., 2002. Detection of Earthquake Damaged Areas from Aerial Photograph by Using Color and Edge Information. *Proceedings of the Fifth Asian Conference on Computer Vision,* pp. 27-32.

Mitomi, H., Yamazaki, F. and Matsuoka, M., 2000. Automated Detection of Building Damage due to Recent Earthquakes Using Aerial Television Images. *21st Asian Conference on Remote Sensing,* Vol. 1, pp. 401-406.

San, B.T., 2002. Detecting Earthquake Induced Changes from Space and Aerial Images. Unpublished Master Thesis, Graduate School of Natural and Applied Sciences, Geodetic and Geographic Information Technologies, Middle East Technical University, Ankara, TURKEY.

Shafarenko, L., Petrou, M. and Kittler, J., 1997. Automatic Watershed Segmentation of Randomly Textured Color Images. *IEEE Trans. Image Processing,* 6(11), pp. 1530-1544.

Sonka, M., Hlavac, V. and Boyle, R., 1998. *Image Processing, Analysis, and Machine Vision,* 2nd Edition, Brooks Cole, USA, pp. 186-188.

Turker, M. and San, B.T., 2003. SPOT HRV data analysis for detecting earthquake-induced changes in Izmit, Turkey. *International Journal of Remote Sensing*, 24(12), pp. 2439-2450.

Turker, M. and Cetinkaya, B., in press. Automatic detection of earthquake damaged buildings using DEMs created from pre- and post-earthquake stereo aerial photographs. *International Journal of Remote Sensing*.

Turker, M. and San, B.T., in press. Detection of collapsed buildings caused by the 1999 Izmit, Turkey earthquake through digital analysis of post-event aerial photographs. *International Journal of Remote Sensing*.

Vincent, L. and Soille, P., 1991. Watersheds in digital spaces: an efficient algorithm based on immersion simulations. *IEEE Transactions on Pattern Analysis and Machine Intelligence,* 13(6), pp. 583-598.